Available online at www.sciencedirect.com

ScienceDirect

Procedia CIRP 82 (2019) 172–177

www.elsevier.com/locate/procedia

17th CIRP Conference on Modelling of Machining Operations

FEM simulation of micromilling of CuZn37 brass considering tool run-out

Andrea Abeni[a], Ceretti Elisabetta[a], Özel Tugrul[b], Attanasio Aldo[a]*

[a]*University of Brescia, Via Branze 38, 25123 Brescia, Italy*
[b]*Rutgers University, Industrial & Systems Engineering, Piscataway, New Jersey, USA*

* Corresponding author. Tel.: +39-030-371-5584; fax: +39-030-370-2448. *E-mail address:* aldo.attanasio@unibs.it

Abstract

Micro-milling process of CuZn37 brass is considered important due to applications in tool production for micro replication technology. Variation in material properties, work material adhesion to tool surfaces, burr formation, and tool wear result in loss of productivity. Chip shapes together with localized temperature, plastic strain, and cutting forces during micro milling process can be predicted using Finite Element (FE) modelling and simulation. However, tool-workpiece engagement suffers from tool run-out affecting process performance in surface generation. This work provides experimental investigations on effects of tool run-out as well as process insight obtained from 3D FE simulations with and without considering tool run-out. Scanning electron microscope (SEM) observation of the 3D chip shapes demonstrates ductile deformed surfaces together with localized serration behavior. FE simulations are utilized to investigate the effects of cutting speed on cutting forces. Cutting force and chip morphology results from simulations are compared with force measurements, and actual chip morphology acquired by SEM revealing reasonable agreements.

Peer-review under responsibility of the scientific committee of The 17th CIRP Conference on Modelling of Machining Operations

Keywords: Micro machining; Finite element method (FEM); Force

1. Introduction

The demand for microproducts has been continuously increasing in biomedical, automotive, aerospace and electronics industries [1]. Among different processes commonly used, micro cutting and micro milling provide high economic efficiency due to high material removal rates. Tool diameters are typically smaller than 1 mm, tool edge roundness is about few microns, and the chip thickness has the same order of magnitude with edge roundness [2]. At this length scale, ploughing, size effect, burr formation, rapid tool wear, higher than expected cutting forces and tool run-out, which are the most common micro milling related issues [3-5], cannot be neglected. Tool run-out is certainly the most important issue causing geometrical inaccuracies [3-5]. This phenomenon occurs due to the sum of the geometrical displacements of the tool axis, the spindle axis, and the tool-holder axis from the ideal axis of rotation [6]. The ratio between this offset and the feed per tooth could be easily high in high speed micro milling. The deviation of the tool edge trajectories involves an asymmetric cutting condition. A change of undeformed chip thickness, a load imbalance between the flutes, a decrease of the tool life and a reduction in workpiece quality are the main consequences of tool run-out.

The development of a good model for describing cutting operation on a micro scale is essential to understand how all process variables influence the product final quality. In fact, the traditional experimental approach run into several difficulties at this scale. Measuring tool temperature and tool wear, evaluating chip morphology and determining the cutting force values are challenging tasks. Finite Element (FE) simulations can be applied to predict these process variables reasonably well, to analyse the generated surfaces and to optimize the machining parameters.

In this study a complete 3D FE model for orthogonal milling is presented. Material behaviour in high deformation rate, hardening, and thermal softening are all considered. Cutting forces and chip morphology obtained from simulations are

Peer-review under responsibility of the scientific committee of The 17th CIRP Conference on Modelling of Machining Operations
10.1016/j.procir.2019.04.011

compared with experimental results for model validation. Micro milling tests are properly designed to obtain an orthogonal cutting configuration and to allow the comparison with FE predictions. The force measurement system has been tested for accuracy on the load cell to ensure its validity for the desired bandwidth [7].

2. Experimental tests

Full immersion micro milling of brass (CuZn37) was performed by using the ultra-precision 5 axes machining center Kern Pyramid Nano (precision of ±0.3 µm). The experimental setup (tool and workpiece geometries, positioning and movements) is illustrated in Fig. 1. Prismatic workpiece (30 mm x 26 mm x 5 mm) is blocked between two Aluminum brackets and is fixed on three components load cell (Kistler 9317C) with four bolts. Two machining operations were executed; (i) roughing to prepare a thin wall on the workpiece, and (ii) orthogonal milling of the thin walled workpiece. After roughing, the workpiece was heat-treated for stress relieving. FE simulations only concern the second operation. A workpiece with 144 µm ± 6 µm thin wall was obtained by using four-flutes 6 mm diameter end mills. Two-flute micro end mills with a rake angle of $\gamma = 0°$ and a helix angle of $\beta=0°$ from SECO company (103L008R005-MEGA-64-T) were used to cut the thin wall without engaging the tool bottom under dry conditions. Tool material was tungsten carbide with (Ti,Al)N coating.

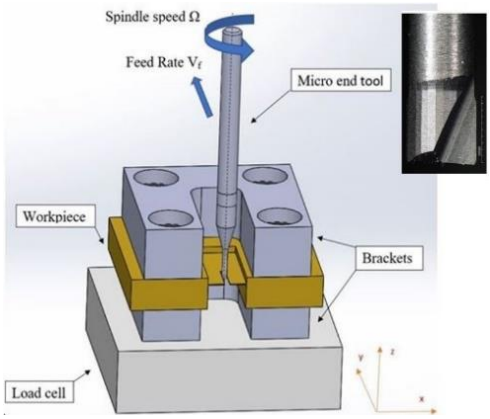

(a)

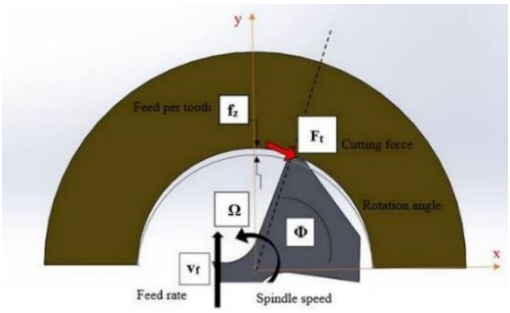

(b)

Fig. 1. (a) Orthogonal milling process with thin wall cutting in 3D configuration, (b) 2D configuration with zero helix angle micro end mill.

Tool geometrical details were measured using 3D digital optical microscope Hirox RH-2000 (measurement accuracy of 0.8 µm). The tool diameter was measured as $\Phi = 782$ µm ±4 µm and tool edge radius was measured as $r_\beta = 4.7$ µm ±0.4 µm. Only the side cutting edge of the tool was engaged with the workpiece. Cutting conditions allow machining to be considered approximately as orthogonal cutting.

Different cutting speeds were used with an aim of investigating their influence on tool run-out and cutting force values. A new tool was used for each test to avoid tool wear effects. Tool advance per rotation in x-direction was kept equal to 10 µm/tooth. Process parameters are summarized in Table 1.

During machining some chip samples were collected and then investigated using a scanning electron microscope (SEM).

A force measurement and data acquisition system that consists of a piezoelectric 3-component force sensor (Kistler 9317C) connected to charge amplifiers (Kistler 5015A) which receive as input three charge signals proportional to the cutting force and return amplified voltage signals as output was used. The force measuring system accuracy is equal to 0.1 N [6].

In micro milling processes, high spindle speed is commonly utilized to overcome the very small feed rate and to maintain adequate productivity [7]. Since the cutting force signals fluctuation is equal to few Newton in few milliseconds the sampling rates must be high to avoid aliasing distortions. In this work, the maximum tooth passing frequency was 1 kHz (as indicated in Table 1) and the sampling rate was fixed at 50 kHz. Furthermore, a limited bandwidth could distort the force signals, as discussed in [3, 4 and 7]. When tooth passing frequencies overlap the load cell natural frequencies, the ideal condition of unity gain and low phase delay is not guaranteed. The modal parameters of the clamping system (dynamometer fixed on machining center, workpiece, and brackets) were detected using impact testing. The measured natural frequencies of the clamping system (Fig. 2) decrease from 5000 Hz (i.e. the natural frequency of the load cell) to 2145 Hz for x-direction and 2192 Hz for y-direction always remaining higher than the maximum tooth passing frequency of 1000 Hz.

Table 1. Micro milling process parameters.

Cutting parameters	Test 1	Test 2	Test 3
Cutting Speed, v_c [m/min]	50	62.5	75
Tooth passing frequency [Hz]	664	848	1000
Axial depth of cut, a_p [µm]	139	150	143

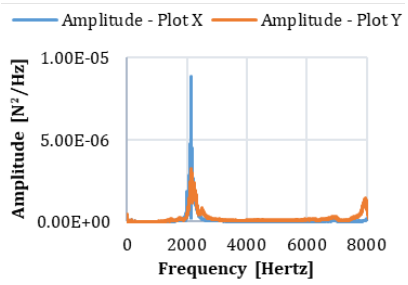

Fig. 2. FRF analysis of natural frequency tested on the entire system.

3. FEM simulation

Finite Element simulation of micro milling was developed using the Lagrangian FE software Deform-3D, performing a thermo-mechanical analysis. A finite element model in 3D was developed instead of a 2D model to capture the 3D chip formation and a more accurate representation of the micro milling process in the simulation results. Simulations are divided into two groups: (i) without considering run-out, and (ii) with tool run-out.

The 3D FE model includes a visco-plastic workpiece and a rigid tool. Fig. 3a shows the simulation set-up as summarized below.

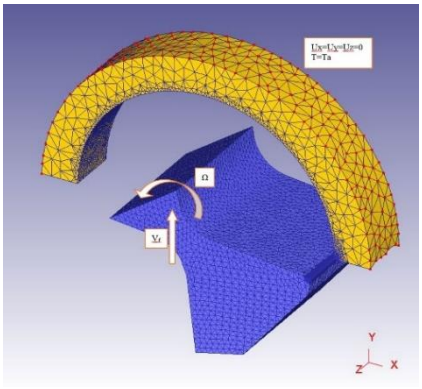

(a)

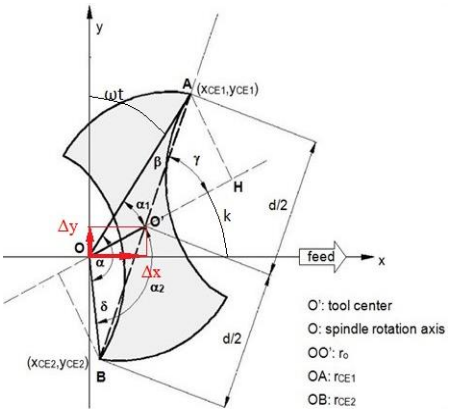

(b)

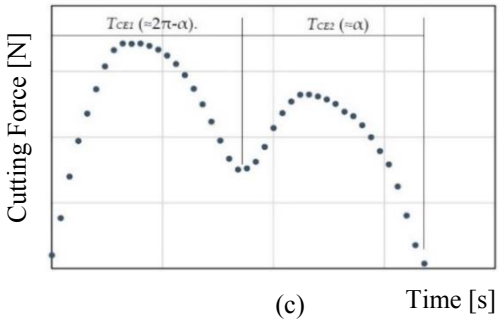

(c)

Fig. 3. Micro milling: (a) FEM 3D model; (b) configuration with run-out; (c) typical signal of cutting force for a two-flute micro end mill with run-out.

At the beginning of the simulation, workpiece mesh has about 44,000 tetrahedral elements. This number was increased up to 200,000 to ensure a high-quality mesh. A minimum element size was kept constant as 1.3 µm. The highest mesh density region was placed around the tool-workpiece contact zone and allowed to follow the chip developed by the milling process. The heat generated by the workpiece deformation was allowed to transfer along the tool path surface and the lateral surfaces. The external surface temperature was fixed at 20°C.

The CuZn37 material constitutive model was implemented by using Johnson-Cook (J-C) law. The flow stress is defined as shown in Eq. (1):

$$\sigma = [A + B \cdot \varepsilon^n]\left[1 + C\, ln\frac{\dot{\varepsilon}}{\dot{\varepsilon}_0}\right]\left[1 - \left(\frac{T-T_0}{T_m-T_0}\right)^m\right] \quad (1)$$

Where σ is the flow stress, ε is the true strain, $\dot{\varepsilon}$ is the true strain rate, $\dot{\varepsilon}_0$ is reference true strain rate, T is the workpiece temperature, T_m is the material melting temperature (T_m = 916°C), T_0 is the room temperature (T_0 = 20°C). The J-C model constants [8] are shown in Table 2.

Table 2. Johnson-Cook model constants. [8].

Model constants	A	B	C	n	m
Values	112	505	0.009	0.42	1.68

Tool geometry reproduces the SECO tool 103L008R005-MEGA-64-T. It was designed only with one flute in order to reduce the number of mesh element and to speed up the simulation. The tool was meshed into 210,000 tetrahedral elements with a minimum size of 0.8 µm, concentrated around the active tool cutting edge.

For simulations with negligible tool run-out, only one flute cutting was modelled. In the case with considerable tool run-out, cutting with both flutes was simulated in order to underline the differences related to cutting forces and chip morphology between the first and the second edge cuts. In particular, for each tool flute cutting, a simulation was designed changing workpiece geometry and tool movement details by considering tool run-out effects.

In each case, workpiece geometry was designed as a half-ring (external diameter = 1000 µm) with a depth in z-direction of 139 µm for Test 1, 150 µm for Test 2, 143 µm for Test 3 respectively, as measured in experimental tests. The arch-shaped curve represents the undeformed geometry as a result of the previous cut. It was designed using the set of Eqs. (2) for simulations without run-out and set Eqs. (3) for simulations with run-out [9].

$$\begin{aligned} x &= r \cdot \cos(\omega \cdot t) \\ y &= r \cdot \sin(\omega \cdot t) + \frac{f \cdot t}{60} \end{aligned} \quad \text{set of Eq (2)}$$

$$\begin{aligned} x_{CE1} &= r_{CE1} \cdot \cos(\omega \cdot t) && \text{(a)} \\ y_{CE1} &= r_{CE1} \cdot \sin(\omega \cdot t) + \frac{f \cdot t}{60} && \text{(a)} \\ x_{CE2} &= r_{CE2} \cdot \cos(\omega \cdot t + \alpha) && \text{(b)} \\ y_{CE2} &= r_{CE2} \cdot \sin(\omega \cdot t + \alpha) + \frac{f \cdot t}{60} && \text{(b)} \end{aligned} \quad \text{set of Eq (3)}$$

The set of Eqs. (3) shall contain some terms in addition to set of Eqs. (2) in order to consider tool run-out. In Fig. 3b the problem geometry is shown. The symbols r_{CE1} and r_{CE2} are the radii of the first (A) and the second (B) cutting edge and they are equal to the distance between the tool edges (A and B) and the spindle center (O), and α is the phase angle of the cutting edges. The tool run-out model [6] assumes that there is no inclination between the tool and the spindle axes (tilt effects are negligible). The ultra-precision machine tool used in this study is sufficient to hold this assumption.

The values of r_{CE1}, r_{CE2} and α can be obtained from some measurements and the geometrical resolution of the problem illustrated in Figure 3b [6]. The radius of first cutting edge (r_{CE1}) could be directly measured by mean of a microscope as the half of the channel width on the workpiece. But, the uncertainty of the optical measurement at this scale and the high elastic recovery effects of CuZn37 brass do not allow applying the direct measurement. For this reason, a new parameter, namely Δr (i.e. the increment of tool radius due to tool run-out), was introduced. Once Δr value is defined, it is possible to calculate the radius of first cutting edge (r_{CE1}) by using Eq. (6):

$$r_{CE1} = \frac{\overline{AB}}{2} + \Delta r \tag{6}$$

Different values of Δr were used in order to investigate its effect on the simulation outputs (Table 4). The tool diameter (AB in Fig. 3b) was fixed at 0.782 mm as the average of the measurements. Referring to Fig. 3c, it is possible to observe that in presence of tool run-out the cutting time of the first cutting edge (T_{CE1}) is higher than that of the second cutting edge (T_{CE2}). The cutting time of each tooth depends on the cutting-edge phase angle (α), and can be estimated by using Eq. (4) and Eq. (5):

$$T_{CE1} = T \cdot \frac{2\pi - \alpha}{2\pi} \tag{4}$$

$$T_{CE2} = T \cdot \frac{\alpha}{2\pi} \tag{5}$$

where $T = T_{CE1} + T_{CE2}$ is the total cutting period.

To estimate the periods (i.e. T, T_{CE1}, and T_{CE2}) a Matlab script was developed. The filtered Fx experimental force signal was fit by means of a Fourier series utilizing the Curve Fitting application of Matlab. Once defined the fitting curve coefficients, utilizing the Matlab function "fminbnd" it is possible to locate the minima of this curve which correspond to the valleys of the force signal. In this manner the periods T, T_{CE1}, and T_{CE2} are identified and the corresponding values of α can be calculated by using Eq. (5). Periods and α angle for each test are reported in Table 3.

The rest of the run-out parameters (r_0 and γ in Fig. 3b) can be determined through trigonometry. By using law of sines, β and δ were determined. Then, with law of cosines, the radius of the second cutting edge ($r_{CE2} = \overline{OB}$) was calculated too. Run-out length ($r_0 = \overline{OO'}$) can be determined by using law of cosines on triangle OO'B. Once the run-out parameters have been calculated, it is possible to calculate how to offset the tool center compared to the spindle center for FE simulation purposes.

Table 3. Tool run out parameters.

Tool run-out parameters	Test 1	Test 2	Test 3
Ω [RPM]	19920	24960	30000
T_{CE1} [ms]	1.5202	1.218	1.0001
T_{CE2} [ms]	1.4919	1.1997	0.9999
α [°]	178.311	178.600	179.986

The distance between O and O' (i.e. r_0) was decomposed in x and y components, called Δx and Δy. Because of rotating tool movement, Δx(t) and Δy(t) change in time and can be calculated as:

$$\Delta x(t) = r_0 \cdot \cos\kappa \tag{7}$$

$$\Delta y(t) = r_0 \cdot \sin\kappa \tag{8}$$

where the time dependent angle κ can be calculated with Eq. (9), obtained by a geometrical analysis of Fig. 3b:

$$\kappa(t) = \frac{\pi}{2} - \alpha_1 - \omega \cdot t \tag{9}$$

κ(t) depends also on angle α_1, which can be obtained by Eq. (10).

$$\alpha_1 = arcsin\left[\frac{r_0 + \frac{d}{2}\cos\gamma}{r_{CE1}}\right] \tag{10}$$

These results were used for both workpiece design and tool center shift compared to spindle center. Eqs. (3a) were used to design the workpiece profile in the simulation of the passes where the tool is engaged with r_{CE2} (tool edge B is working) and Eqs. (3b) were used when the tool was engaged with r_{CE1} (tool edge A is working). In FE simulations without run-out, tool was positioned with its center O' overlapped to the spindle rotation center O and then a rotation around O ≡ O' was set. In FE simulations with tool run-out, tool center O' was initially offset by Δx(t*) and Δy(t*), calculated at different time (respectively t_1* and t_2*) for simulating the tool edge A and tool edge B: the first edge starts to engage the workpiece when $\omega \cdot t_1^* = 0$; the second edge starts to engage the workpiece when $\omega \cdot t_2^* = 2\pi - \alpha$. Then the tool rotation was set around spindle center O, from 0° to 180°. In Table 4, the parameters of the FE simulation designs considering tool run-out are summarized.

As previously explained, the movement was assigned to the tool, using speeds according to the experimental values. Tool boundary conditions allow to transfer heat throughout the entire body. The heat transfer conduction coefficient between tool and workpiece plays a key role in chip formation dynamics [10, 11]. This parameter was set equal to 10^5 N s^{-1} mm^{-1} °C^{-1}. It is a higher than usual value, necessary to generate sufficient temperature in the short duration of the simulation (about 0.001 s). Heat exchange is allowed also between the system and the environment. All material properties for the workpiece, the tool, and the coating are given in Table 5.

Table 4. Parameters used for tool run-out simulations.

Values in µm	r_{CE1}=392µm $\Delta r = r_{CE1}$-AB/2=1µm			r_{CE1} = 393 µm $\Delta r = r_{CE1}$-AB/2= 2 µm		
	Test 1	Test 2	Test 3	Test 1	Test 2	Test 3
r_{CE2}	390.08	390.05	390.00	389.06	389.06	389.00
r_0	5.843	4.874	1.001	6.087	5.167	2.000
$\Delta x(t_1^*)$	5.749	4.764	0.04	5.734	4.752	0.044
$\Delta y(t_1^*)$	1.042	1.029	1.00	2.042	2.029	2.000
$\Delta x(t_2^*)$	-5.777	-4.788	-0.04	-5.792	-4.800	-0.045
$\Delta y(t_2^*)$	-0.872	-0.912	-1.00	-1.872	-1.912	-2.000

Table 5. Thermal and mechanical properties of materials.

Properties	CuZn37	WC	(Ti,Al)N
Thermal conductivity ($Ns^{-1}°C^{-1}$)	370	59	Function of T
Heat capacity (Nmm^{-2} $°C^{-1}$)	3.272	15	Function of T
Thermal exp. Coeff.($°C^{-1}$)	2.2e-05	5e-06	9.4e-06
Young's modulus (MPa)	1.1e+05	6.5e+05	6.0e+05
Poisson's ratio	0.33	0.25	0.25

The friction between workpiece and tool was modelled using the hybrid model, which considers both sticking and sliding contacts [10, 11]. Shear friction factor m was set equal to 0.9 and Coulomb friction coefficient μ was fixed at 0.4.

4. Comparison of predicted cutting forces and chip shapes

Simulations achieve a good prediction of the experimental forces. For simulation without considering tool run-out, Test 2 is used because in this experiment the difference of cutting force between the tool teeth was minimum (see Fig. 4). In Fig. 4a and Fig. 4b, a comparison between simulated and experimental results for Test 2 is presented. Lower and upper bounds of experimental charts are built with a confidence level equal to 68%.

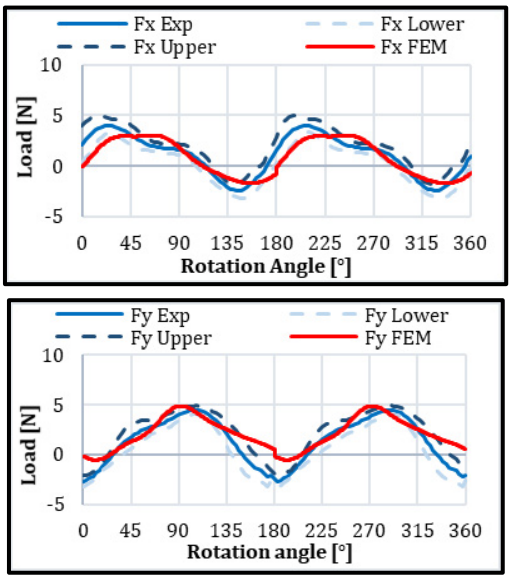

Fig. 4. Comparison of predicted and experimental forces (no run-out).

In Fig. 5a, the values of load peaks (experimental and simalted under different value of Δr) are considered for Fx and Fy for each cutting edge (EA and EB) and for each test

Upper and lower bounds are necessary to check the overlapping between FE and experimental results taking into account the variability of the experimental data. In fact, they are calculated as an average value on several tool rotations. In Test 1 and Test 2, there is a good match on both force components, and better results deals with the value of Δr of 2 µm. The entire force plots for Test 1 in this configuration (Δr = 2 µm) are shown in Fig. 5. However, model validity for Test 3 is not satisfactory. Experimental loads for this test are significantly higher than the force values of Test 1 and Test 2 (see Fig. 6). A possible explanation for this result can be related to the experimental set-up. The thin-wall cut with higher cutting speed undergoes to greater vibrations which affect the force measurements. Furthermore, considering the simulation results, it is well-known how, at the high cutting speed (i.e. higher strain-rates), the material constitutive law expressed by Johnson-Cook model underestimates the actual flow stresses and, as a consequence, the predicted cutting forces.

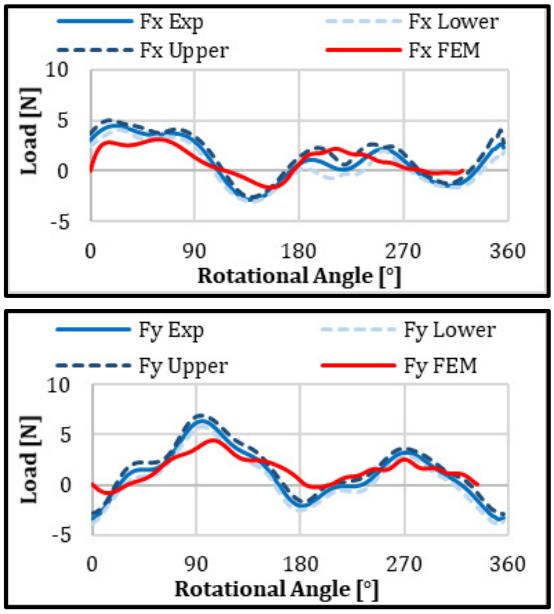

Fig. 5. (a) Comparison between experimental forces and simulations results for Test 1 (run-out effects considered).

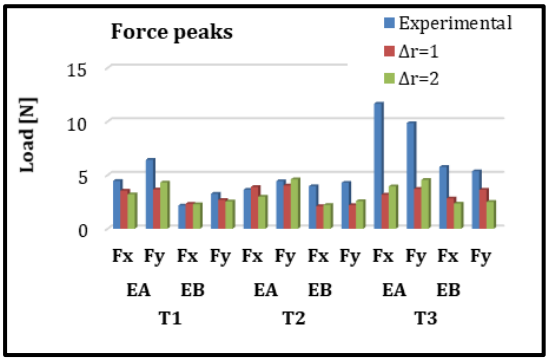

(c)

Fig. 6. Comparison between experimental forces and simulations results for each test.

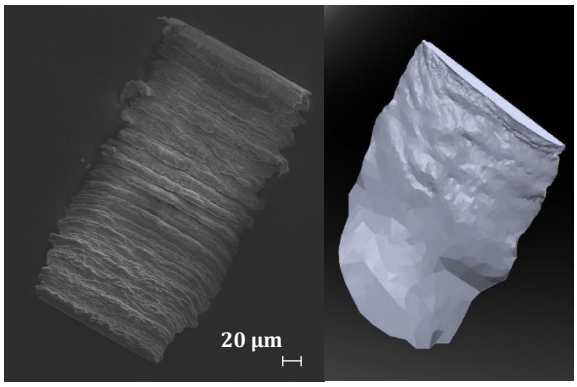

Fig. 7. Comparison between a SEM image of a chip sample (a) and a part of the simulated chip shape (b) for Test2.

A possible explanation for this result can be related to the experimental set-up. The thin-wall cut with higher cutting speed undergoes to greater vibrations which affect the force measurements. Furthermore, considering the simulation results, it is well-known how, at the high cutting speed (i.e. higher strain-rates), the material constitutive law expressed by Johnson-Cook model underestimates the actual flow stresses and, as a consequence, the predicted cutting forces.

Reasonably good results are obtained for the chip shapes from the FE simulations. Fig. 7 shows an exemplary comparison between simulated and experimental chip shapes. It is possible to observe that the simulation is able to predict the chip segmentation as well.

5. Conclusion

This study presents an experimental and Finite Element simulation based investigations about the effect of tool run-out on 3D orthogonal micro milling configuration. The size of the tool run-out deviation does not result in direct connection to the cutting speed and it remains in the magnitude order of few micrometres. The cutting forces are significantly influenced by tool run-out and this effect can be reliably predicted by the FE simulation model coupled with tool run-out. This methodology relies on measurement of tool run-out from orthogonal micro-milling tests and on measuring cutting forces generated by two flutes of the micro end mill. It was shown that while FE simulations accurately predict cutting forces in the presence of no tool run-out effect, the improved FE simulation methodology by considering tool motion with calculated tool run-out results in reasonably good cutting force predictions as well. It is also noted that the qualitative comparison of predicted chip flow and chip shapes is reasonably good results. A more quantitative analysis of experimental chip samples as compared with predicted chips is required for further validating the mechanism of chip formation when considering tool run-out in micro milling processes.

References

[1] Dornfeld D, Mina S, Takeuchi Y. Recent Advances in Mechanical Micromachining. CIRP Annals - Manufacturing Technology 2006; 55:745–768.
[2] Bissacco G, Hansen HN, Slunsky J. Modelling the cutting edge radius size effect for force prediction in micro milling. CIRP Ann. Manuf. Technol. 2008; 57:113–116.
[3] Park SS, Malekian M. Mechanistic modeling and accurate measurement of micro end milling forces. CIRP Ann. Manuf. Technol 2009; 58:49–52.
[4] Malekian M, Park SS, Jun MBG. Modeling of dynamic micro-milling cutting forces. Int. J. Mach. Tools Manuf 2009; 49:586–598.
[5] Altintas Y, Jin X. Mechanics of micro-milling with round edge tools. CIRP Annals - Manufacturing Technology 2011; 60 (1):77-80.
[6] Attanasio A. Tool run-out measurement in micro milling. Micromachines 2017; 8:221.
[7] Korkmaz E, Gozen BA Bediz B, Ozdoganlar OB. Accurate measurement of micromachining forces through dynamic compensation of dynamometers. Precision Engineering 2017; 49:365–376.
[8] Johnson GJ, Cook WH. A constitutive model and data for metals subjected tool large strains, high strain rates and high temperatures. Proc. 7th international Symposium on Ballistics1983; 541-547.
[9] Attanasio A, Garbellini A, Ceretti E, Giardini C. Force modelling in micromilling of channels. International Journal of Nanomanufacturing 2015; 11(5-6):275-296.
[10] Özel T, Olleak A, Thepsonthi T. Micro milling of titanium alloy Ti-6Al-4V: 3-D finite element modeling for prediction of chip flow and burr formation. Production Engineering 2017; 11 (4–5):435–444.
[11] Thepsonthi T, Özel T. 3-D Finite Element Process Simulation of Micro-end Milling Ti-6Al-4V Titanium Alloy: Experimental Validations on Chip Flow and Tool Wear. Journal of Materials Processing Technology 2015; 221:128–145.